International Journal of Heat and Mass Transfer 63 (2013) 301–312

Contents lists available at SciVerse ScienceDirect

International Journal of Heat and Mass Transfer

journal homepage: www.elsevier.com/locate/ijhmt

Heat and mass transfer and chemical transformation in a cerium nitrate droplet

Binita Pathak [a], Saptarshi Basu [a], Ranganathan Kumar [b,*]

[a] *Indian Institute of Science, Bangalore, India*
[b] *University of Central Florida, Orlando, USA*

ARTICLE INFO

Article history:
Received 11 November 2012
Received in revised form 2 April 2013
Accepted 6 April 2013
Available online 30 April 2013

Keywords:
Acoustic levitation
Heat and mass transfer
Chemical reaction
Droplet vaporization
Nanoceria
Droplet agglomeration

ABSTRACT

This paper deals with the thermo-physical changes that a droplet undergoes when it is radiatively heated in a levitated environment. The heat and mass transport model has been developed along with chemical kinetics within a cerium nitrate droplet. The chemical transformation of cerium nitrate to ceria during the process is predicted using Kramers' reaction mechanism which justifies the formation of ceria at a very low temperature as observed in experiments. The rate equation modeled by Kramers is modified suitably to be applicable within the framework of a droplet, and predicts experimental results well in both bulk form of cerium nitrate and in aqueous cerium nitrate droplet. The dependence of dissociation reaction rate on droplet size is determined and the transient mass concentration of unreacted cerium nitrate is reported. The model is validated with experiments both for liquid phase vaporization and chemical reaction. Vaporization and chemical conversion are simulated for different ambient conditions. The competitive effects of sensible heating rate and the rate of vaporization with diffusion of cerium nitrate is seen to play a key role in determining the mass fraction of ceria formed within the droplet. Spatially resolved modeling of the droplet enables the understanding of the conversion of chemical species in more detail.

1. Introduction

Spray drying is employed extensively in chemical, pharmaceutical and ceramic industries to generate particles with tailored morphologies and microstructures by controlled vaporization of functional droplets containing dissolved salts or nanosuspensions. Solvent depletion from the droplet surface at specified rate leads to particle accumulation and consequent agglomeration. In the case of droplets containing dissolved salts (e.g. cerium nitrate), vaporization induced solute accumulation is followed by precipitation of nanosized particles which subsequently react chemically to produce stable nano-phase structures (e.g. nano-ceria). These nano-ceramic particles are widely used in powder technology, coating industry, catalysis as well as in solid oxide fuel cells. Nano ceria coatings are found to be excellent in resisting corrosion even at very high temperatures [1,2]. Hence the study of a single functional droplet containing cerium nitrate (in dissolved phase) that undergoes a series of thermo-physical processes (vaporization, accumulation and precipitation) and vigorous chemical reactions leading to the formation of spatially non-uniform ceria is of paramount importance [3–7].

Various models on the heating of single and multi-component single phase droplets are found in the literature [3–7]. Vaporization of liquid along with migration of solute within the droplet in a convective environment is governed by liquid phase heat and mass transport mechanisms coupled with the outer flow field. Formation of ceria from cerium nitrate droplets can be achieved through a variety of processes that either involve very rapid heat transfer (as in plasma) or slow heating (as in spray drying). For example, different stages involved in solution precursor plasma spray (SPPS) process for production of nano ceria coatings using cerium nitrate droplet as precursor was modeled by Saha et al. [8]. In this endothermic reaction, cerium nitrate dissociates to ceria and releases other gases [2]:

$$\mathrm{Ce(NO_3)_3} \rightarrow \mathrm{CeO_2} + \mathrm{NO_X} - 208\ \mathrm{J/gm}$$

Preparation of ceria by gradual dehydration and thermal decomposition of cerium nitrate can also be found in [9,10]. The anhydrous cerium nitrate ($\mathrm{Ce\,(NO_3)_3}$) is experimentally found to dissociate into ceria ($\mathrm{CeO_2}$) at a high temperature range of 230°C to 360°C [10].

The transport phenomenon during heating of cerium nitrate droplet by CO_2 laser was studied experimentally using a pendant droplet [11] and a levitated droplet [12]. Saha et al. [12] showed that for 500 micron droplets, the formation of ceria when irradiated by a laser occurs at a temperature of about 70°C. TEM

---

* Corresponding author. Tel.: +1 407 823 4389; fax: +1 407 823 0208.
E-mail address: ranganathan.kumar@ucf.edu (R. Kumar).

0017-9310/$ - see front matter © 2013 Elsevier Ltd. All rights reserved.
http://dx.doi.org/10.1016/j.ijheatmasstransfer.2013.04.008

Nomenclature

a_λ	liquid absorption coefficient
A	Arrhenius rate constant
A_e	Absorption efficiency factor
B_M	spalding mass transfer number$=\left(\frac{\chi_{v,s}-\chi_{v,\infty}}{1-\chi_{v,s}}\right)$
B_T	spalding heat transfer number$=\frac{C_{P,F}(T_\infty-T_s)}{h_{fg}+(Q_L/\dot{m})}$
$C_{P,F}$	specific heat constant of vapor phase (J/kg K)
$C_{P,L}$	specific heat constant of liquid phase (J/kg K)
d	diameter of cerium nitrate particle (m)
d_0	diameter of droplet (m)
D_{AB}	vapor phase mass diffusivity (m^2/sec)
D_{12}	liquid phase mass diffusivity (m^2/sec)
E_a	activation energy (kJ/mol)
h_{fg}	latent heat of vaporization (J/kg)
I	intensity of radiations (MW/m^2)
k_b	Boltzmann constant (m^2kg/s^2 K)
k_g	thermal conductivity of vapor phase (W/m K)
k_L	thermal conductivity of liquid phase (W/m K)
Le_L	Lewis number, $\frac{k_L}{\rho_L C_{pL} D_{12}}$
$\dot{m}$	rate of mass flow due to vaporization (kg/s)
$\dot{m}_p$	mass source/sink term (kg/m^3sec)
$\bar{m}_p$	non-dimensionalized mass source/sink term
M_μ	frequency parameter, $\sqrt{2\pi f \frac{r_s^2}{\nu_{air}} \frac{\mu_{air}}{\mu_{drop}}}$
Nu_o	Nusselt number
Nu^*	Nusselt number modified with surface blowing effect
Pe_L	liquid phase Peclet number
Pr	Prandtl number $\left(=\frac{\gamma_v}{\propto_v}\right)$
$\dot{q}_s$	volumetric heat sink (J/m^3s)
$\bar{q}_s$	non-dimensional heat sink
Q	heat absorbed (W/m^3)
Q_L	heat delivered into the droplet (W)
$\dot{Q}$	rate of heat generated with radiation (W)
$\dot{Q}_r(\eta)$	non-dimensional radiative heat source
r	radial co-ordinate
r_{ppt}	radius of cerium nitrate precipitate (m)
r_s	droplet radius at any time instant (m)
$\bar{r}_s=\frac{r_s}{r_0}$	non-dimensionalized size of droplet
R	universal gas constant (J/kg K)
Re	Reynolds number
R_i	refractive index
Sc	Schmidt number
Sh_o	Sherwood number
Sh^*	Sherwood number modified with surface blowing effect
t	simulation time
t_v	simulation timescale of vaporization (secs)
T	temperature (K)
T_0	initial temperature of droplet (K)
T_∞	temperature of surrounding flow field (K)
T_s	temperature at surface of droplet (K)
$\bar{T}$	non-dimensionalized temperature, $\frac{T-T_0}{T_0}$
V_r	radial component of internal flow field velocity (m/s)
V_θ	tangential component of internal flow field velocity (m/s)
V_{drop}	volume of droplet
$\bar{V}_r$	non-dimensionalized velocity in radial direction
$\bar{V}_\theta$	non-dimensionalized velocity in tangential direction

Greek characters

α_L	liquid phase thermal diffusivity (m^2/sec)
α_v	vapor phase thermal diffusivity (m^2/sec)
ρ_L	liquid density (kg/m^3)
ρ_g	gas phase density (kg/m^3)
τ	non-dimensionalized time, $\alpha_L \frac{t}{r_0^2}$
η	non-dimensionalized spatial co-ordinate, $\frac{r}{r_s}$
ν_{air}	kinematic viscosity of air (m^2/sec)
ν_v	kinematic viscosity of vapor phase (m^2/sec)
μ_{air}	dynamic viscosity of air (Pa.s)
μ_{drop}	dynamic viscosity fluid inside droplet (Pa.s)
μ_L	dynamic viscosity of liquid (Pa.s)
χ_0	initial concentration of un-dissolved particles in the droplet
χ_p	concentration of each species (cerium nitrate and ceria) at any time instant in the droplet
$\chi_{v,\infty}$	mass fraction of vapor phase far away from droplet
$\chi_{v,s}$	mass fraction of vapors at droplet surface
$\bar{\chi}_p$	non-dimensionalized species concentration, $\frac{\chi_p-\chi_0}{\chi_0}$
θ	tangential co-ordinate
λ	mean free path (m)

(Transmission Electron Microscope) images displayed in Fig. 1 shows the formation of nitrogen oxide bubbles (byproducts of chemical reaction), and also nanoceria from the chemical reaction [12]. Wendlandt [13] showed that hexahydrate cerium nitrate sample in bulk (not dissolved in small droplets) only starts drying out at 80°C which continues until CeO_2 is formed at about 450°C for low heating rate.

The experiments showing dissociation reaction at high temperatures are usually performed with bulk amounts of cerium nitrate. The salt is first dehydrated and the mass decomposed is then studied using Thermo Gravimetric Analysis (TGA). However, in real life systems like spray drying, spray pyrolysis and plasma spray processes [8,11,12] (for thermal barrier coatings) droplets containing dissolved quantities of cerium nitrate is decomposed to ceria on the fly and exhibit fast kinetics. In fact, in plasma/flame spray processes, the kinetic decomposition occurs within 0.1-2 ms. The decomposition timescale is however larger in spray drying (usually of the order of seconds).

A levitated droplet is free from any surface contact. Acoustic levitation of droplets with radiative heating provides a unique opportunity to study diameter regression, agglomeration, precipitation, and chemical reaction in details. These experimental efforts have been reported earlier by our group [14–16]. Our modeling efforts [7,8] have mostly focused on the heat and mass transport dynamics. Agglomeration and heat and mass transport were modeled for nanosilica droplets [17]. This work aims to bridge the gap between vaporization and chemical reaction in a levitated cerium nitrate droplet.

In this work, the heat and mass transport processes of an evaporating acoustically levitated cerium nitrate droplet are reported along with the chemical kinetics of the formation of ceria. A cerium nitrate droplet (aqueous solution of cerium nitrate at certain volume concentration) is heated both radiatively (using laser) and convectively that lead to vaporization, temperature rise and consequent diameter regression. The spatial distribution of ceria within the droplet is shown to be dependent on reaction rate, temperature field and the initial cerium nitrate concentration profile. The uniqueness in the model is its ability to incorporate the heat and mass transport within the vaporizing droplet and also allow for chemical kinetics in the transformation of cerium nitrate to ceria. The reaction rate has been adopted from Kramers' model [18] and modified for a droplet.

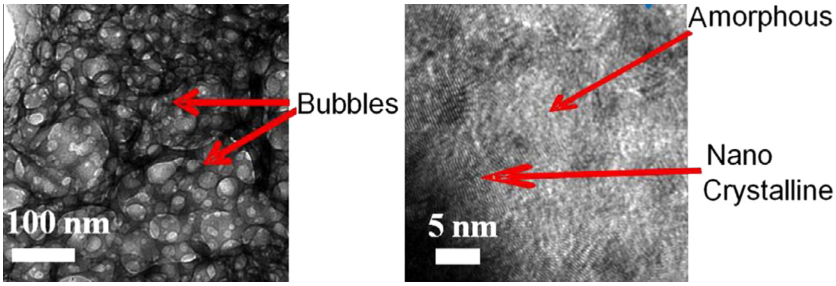

Fig. 1. TEM images indicating bubbles due to chemical reaction and formation of nano crystalline ceria within the laser heated droplet [12] (reproduced with permission).

2. Numerical modeling

The model is simulated with a hydrated cerium nitrate droplet which is acoustically levitated and heated with monochromatic irradiation using CO_2 laser (intensity, I = 0.45 MW/m^2). The droplet of initial size (d_0) of 500 micron was levitated in a convective environment maintained at a temperature (T_{str}) of 525 K and 425 K and at a gas phase velocity (U_{str}) of 1.6 m/s. The evaporation model is similar to that described in [6,19]. Heat input from the hot air through convection along with the heat absorbed due to radiation increases the temperature of the droplet which begins to vaporize. Due to vaporization, the droplet size (r_s) decreases, increasing the concentration of cerium nitrate which then precipitates. The energy needed for subsequent reaction is provided by the heat flux (radiative and convective), which results in the dissociation of cerium nitrate into ceria. The numerical procedure is shown in Fig. 2.

2.1. Flow due to acoustic streaming

The droplet is stabilized at an antinode of the acoustic standing wave and accordingly the internal recirculation pattern generated in the droplet due to outer streaming is simulated by the stream function ($\widehat{\Psi}$) theoretically deduced by Rednikov et al. [20]:

$$\begin{aligned}\widehat{\Psi} &= \bar{k}\sin(\bar{k}z_0)\cos(\bar{k}z_0)\frac{\sqrt{2}}{24}M_\mu(r^2-r^4)(1-\bar{\mu}^2)+\cos^2(\bar{k}z_0)\\ &\times\frac{9\sqrt{2}}{160}M_\mu(r^3-r^5)\bar{\mu}(1-\bar{\mu}^2)-\bar{k}\sin(\bar{k}z_0)\cos(\bar{k}z_0)\\ &\times\frac{3\sqrt{2}}{112}M_\mu(r^4-r^6)(5\bar{\mu}^2-1)(1-\bar{\mu}^2) \qquad (1)\end{aligned}$$

where $\bar{k}$ is the non-dimensional acoustic wave number, M_μ the frequency parameter and $\bar{\mu} = \cos\theta$. r and θ are the spherical co-ordinates measured from the droplet center located at $z = z_0$. The internal recirculation pattern developed affects the transport phenomena within the droplet.

The outer flow creates shear stress at the droplet surface and the skin friction coefficient which is a function of the Reynolds number $Re = 2\rho_\infty U_{str} r_s/\mu_g$ is correlated as [21]:

$$C_F = \frac{12.69}{Re^{-2/3}(1+B_M)} \qquad (2)$$

ρ_∞ and μ_g are the density and dynamic viscosity of the surrounding gas phase respectively and B_M is the Spalding mass transfer number.

2.2. Radiative and convective heat transfer

The droplet is assumed to be semi-transparent and volumetrically irradiated with laser intensity I (W/m^2), such that the amount of heat absorbed locally is given as [22]:

$$\dot{Q} = \pi r_s^2 I A_e \qquad (3)$$

The absorption efficiency factor, A_e is estimated to be:

$$A_e = \frac{4R_i}{\left(1+R_i^2\right)}\{1-exp(-2r_s a_\lambda)\}, \qquad (4)$$

where, R_i is refractive index and a_λ is the liquid absorption coefficient [22]. a_λ for water based solutions is approximately $10^5\ m^{-1}$ at 10.5 micron wavelength of irradiation (CO_2 laser). R_i is taken to be 1.33.

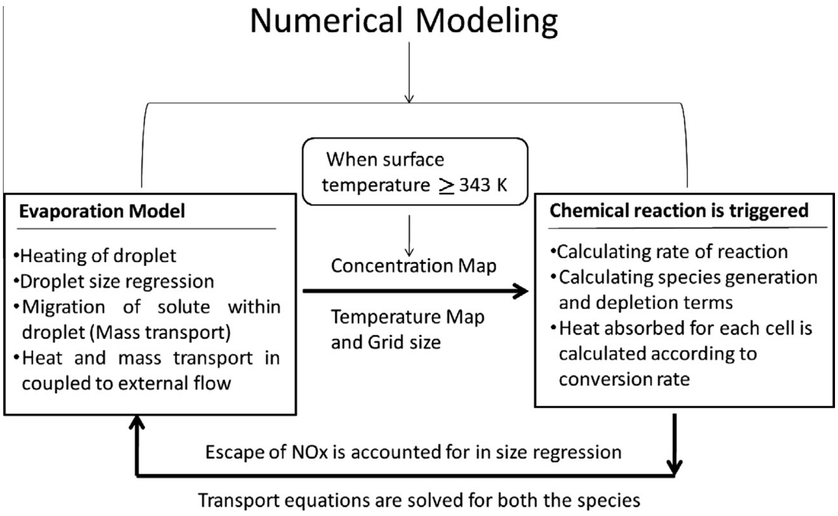

Fig. 2. Schematic of numerical approach.

The heat flow from ambient is calculated using Spalding heat transfer number (B_T) as stated below:

$$Q_{\mathrm{L}} = \dot{m}((C_{\mathrm{P,F}}(T_\infty - T_{\mathrm{s}})/B_{\mathrm{T}}) - h_{\mathrm{fg}}) \tag{5}$$

where $C_{\mathrm{P,F}}$ is the specific heat constant of the vapor phase, T_{s} and T_∞ are temperatures Nu^* at droplet surface and that of the surrounding and h_{fg} is the latent heat of vaporization of the liquid phase.

2.3. Gas phase analysis

All the properties of vapor phase are calculated as a function of average temperature $T = (2T_s + T_\infty)/3$ according to the two-third rule suggested by Hubbard et al. [23]. The gas phase analysis is assumed to be quasi-steady due to the large timescale of mass vaporization and lower mass diffusivity in the vapor phase. With this assumption, Nusselt and Sherwood numbers correlations [24] can be written as:

$$Nu_{\mathrm{o}} = 1 + (1 + RePr)^{1/3} f(Re) \tag{6}$$

$$Sh_{\mathrm{o}} = 1 + (1 + ReSc)^{1/3} f(Re) \tag{7}$$

where, Pr and Sc are the Prandtl and Schmidt numbers respectively. The surface blowing effect due to Stefan flow is taken into account in Nusselt number (Nu^*) and Sherwood number (Sh^*) which are modified accordingly [6,19]:

$$Nu^* = 2 + \frac{Nu_{\mathrm{o}} - 2}{F(B_{\mathrm{T}})} \tag{8}$$

$$Sh^* = 2 + \frac{Sh_{\mathrm{o}} - 2}{F(B_{\mathrm{M}})} \tag{9}$$

Where, $F(B)$ is the universal function to account for the surface blowing effect.

No changes in the droplet are expected due to the fluctuations in the acoustic wave since the acoustic frequency is 100 kHz. Hence, the assumption of quasi-steady gas phase is justified and only the average velocity (U_{str}) of the outer gas flow (in terms of Reynolds number) is used to calculate the transport rates [17]. Accordingly, the momentum equation in the gas phase need not be solved. The mass vaporizing rate in the droplet is then calculated as [6,19]:

$$\dot{m} = 2\pi\rho_{\mathrm{g}} D_{\mathrm{AB}} r_{\mathrm{s}} Sh^* ln(1 + B_{\mathrm{M}}) \tag{10}$$

$$\dot{m} = 2\pi \frac{k_{\mathrm{g}}}{C_{\mathrm{P,F}}} r_{\mathrm{s}} Nu^* ln(1 + B_{\mathrm{T}}) \tag{11}$$

D_{AB} is mass diffusivity of water vapor in air, k_{g} and ρ_{g} are the vapor thermal conductivity and density respectively.

2.4. Liquid phase transport analysis

The droplet is attached to an Eulerian spherical co-ordinate system and an axisymmetric external flow field due to acoustic streaming is considered. The droplet domain is discretized into a number of uniform grids (30, 30) in the radial and tangential directions (r,θ). The governing equations get reduced to two-dimensional energy and species transport Eqs. (12) and (13) which are given in [6,19].

$$\bar{r}_{\mathrm{s}}^2 \frac{\partial \overline{T}}{\partial \tau} + \left(0.5Pe_{\mathrm{L}} \overline{V}_{\mathrm{r}} \bar{r}_{\mathrm{s}} - 0.5\eta \frac{d\bar{r}_{\mathrm{s}}}{d\tau}\right) \frac{\partial \overline{T}}{\partial \eta} + 0.5Pe_L \frac{\overline{V}_\theta \bar{r}_{\mathrm{s}}}{\eta} \frac{\partial \overline{T}}{\partial \theta} = \frac{1}{\eta^2} \frac{\partial}{\partial \eta}\left(\eta^2 \frac{\partial \overline{T}}{\partial \eta}\right) + \frac{1}{\eta^2 \sin\theta} \frac{\partial}{\partial \theta}\left(\sin\theta \frac{\partial \overline{T}}{\partial \theta}\right) + \bar{r}_{\mathrm{s}}^2 \dot{Q}_{\mathrm{r}}(\eta) - \bar{q}_{\mathrm{s}} \tag{12}$$

$$Le_{\mathrm{L}} \bar{r}_s^2 \frac{\partial \bar{\chi}_1}{\partial \tau} + \left(0.5Pe_{\mathrm{L}} Le_{\mathrm{L}} \overline{V}_{\mathrm{r}} \bar{r}_{\mathrm{s}} - 0.5Le_{\mathrm{L}} \eta \frac{d\bar{r}_{\mathrm{s}}}{d\tau}\right) \frac{\partial \bar{\chi}_1}{\partial \eta} + 0.5Pe_{\mathrm{L}} Le_{\mathrm{L}} \frac{\overline{V}_\theta \bar{r}_{\mathrm{s}}}{\eta} \frac{\partial \bar{\chi}_1}{\partial \theta} = \frac{1}{\eta^2} \frac{\partial}{\partial \eta}\left(\eta^2 \frac{\partial \bar{\chi}_1}{\partial \eta}\right) + \frac{1}{\eta^2 \sin\theta} \frac{\partial}{\partial \theta}\left(\sin\theta \frac{\partial \bar{\chi}_1}{\partial \theta}\right) - \bar{m}_1 \tag{13a}$$

$$Le_{\mathrm{L}} \bar{r}_{\mathrm{s}}^2 \frac{\partial \bar{\chi}_2}{\partial \tau} + \left(0.5Pe_{\mathrm{L}} Le_{\mathrm{L}} \overline{V}_{\mathrm{r}} \bar{r}_{\mathrm{s}} - 0.5Le_{\mathrm{L}} \eta \frac{d\bar{r}_{\mathrm{s}}}{d\tau}\right) \frac{\partial \bar{\chi}_2}{\partial \eta} + 0.5Pe_{\mathrm{L}} Le_{\mathrm{L}} \frac{\overline{V}_\theta \bar{r}_{\mathrm{s}}}{\eta} \frac{\partial \bar{\chi}_2}{\partial \theta} = \frac{1}{\eta^2} \frac{\partial}{\partial \eta}\left(\eta^2 \frac{\partial \bar{\chi}_2}{\partial \eta}\right) + \frac{1}{\eta^2 \sin\theta} \frac{\partial}{\partial \theta}\left(\sin\theta \frac{\partial \bar{\chi}_2}{\partial \theta}\right) + \bar{m}_2 \tag{13b}$$

where, $\bar{r}_s = \frac{r_s}{r_0}, \bar{\chi}_p = \frac{\chi_p - \chi_0}{\chi_0}, \overline{T} = \frac{T - T_0}{T_0}$ are dimensionless radius, concentration of each species (cerium nitrate and ceria) present in droplet and temperature. $p = 1,2$ represents cerium nitrate and ceria respectively. $\tau = \alpha_L \frac{t}{r_0^2}$ and $\eta = \frac{r}{r_s}$ are the non-dimensionalized time and co-ordinate in radial direction. r_0, T_0, χ_0 are initial radius, temperature and cerium nitrate concentration in droplet of radius r_{s} at any time instant, α_{L} is liquid phase thermal diffusivity. Pe_L and Le_L are Peclet and Lewis number of the liquid phase. Eq. (13b) is only activated after the onset of chemical reaction and not during the pure vaporization phase. The internal flow field (V_r and V_θ in r and θ directions) in the liquid phase is governed by the outer flow field (given in Eq. (1)). Therefore the momentum equation need not be solved for the liquid phase. $\dot{Q}_{\mathrm{r}}(\eta)$ is the non-dimensional radiative heat source, $\dot{Q}_r(\eta) = Q \frac{r_s^2}{T_o k_L}$ (Q is rate of heat absorbed per unit volume, $Q = \dot{Q} \frac{3}{4\pi r_s^3}$) varying radially inside the droplet. $\bar{q}_{\mathrm{s}} = \dot{q}s \frac{r_s^2}{T_o k_{\mathrm{L}}}$ and $\bar{m}_p = \dot{m}_p \frac{r_s^2}{\chi_0 \alpha_L \rho_L}$ are the non-dimensional heat sink and mass source/sink terms respectively, which are activated once the chemical reaction is triggered and k_{L} and ρ_{L} are the thermal conductivity and density of the nanofluid under consideration. $\dot{q}_s$ is volumetric heat sink (J/m^{3}s) and $\dot{m}_p$ is volumetric mass generation/depletion rate (kg/m^{3}s).

The convective heat flux (Q_L) to the droplet and the mass flow rate ($\dot{m}$) are estimated using B_{M},B_{T},Nu^* and Sh^* in an iterative manner (supplemented with Clausius–Clapeyron equation for estimating vapor pressure) along with Raoult's law (for determination of $\chi_{\mathrm{v,s}}$) and taken into account in the boundary conditions for Eqs. (12) and (13):

At the surface of the droplet ($\eta = 1$),

$$\frac{\partial \overline{T}}{\partial \theta} = 0, \frac{\partial \bar{\chi}_p}{\partial \theta} = 0, \int_0^\pi \frac{\partial \overline{T}}{\partial \eta} \sin\theta d\theta = \frac{Q_L}{2\pi r_s k_L T_0} \ \textit{and}$$

$$\int_0^\pi \frac{\partial \bar{\chi}_w}{\partial \eta} \sin\theta d\theta = \frac{-\dot{m}}{2\pi r_s \rho_L D12 \chi_0}$$

At the center, $(\theta = 0), \frac{\partial \overline{T}}{\partial \theta} = 0$ and $\frac{\partial \bar{\chi}_p}{\partial \theta} = 0$.

Here, k_L and ρ_{L} are the liquid phase thermal conductivity and density, and D_{12} is the mass diffusivity of cerium nitrate and ceria in water. $\bar{\chi}_w = 1 - \bar{\chi}_1 - \bar{\chi}_2$ is the mass fraction of water at the surface. The transient temperature and concentration fields inside the droplet (Eqs. (12) and (13)) are explicitly solved using the modified Du Fort Frankel numerical scheme with second order accuracy in both time and space [17]. The time step is chosen to be $\Delta t_{\mathrm{vap}} = 5 \times 10^{-6}$ s considering the consistency and accuracy of the model and independent of acoustic wave frequency (quasi-steady assumption). The total simulation time is $t_{\mathrm{vap}} = 5$ s when water is vaporized completely. The temperature and concentration at the droplet surface are both considered to be spatially uniform and are solved using boundary conditions as mentioned in [6,19]. Both the energy and species conservation equations are solved for the liquid phase and are coupled with the external flow field (assumed quasi-steady) with continuity conditions at the interfaces along with the correlations for Sh^* and Nu^*. The depletion in droplet size due to vaporization of water (assumed to be equivalent to the evaporation rate of water) is calculated and for each new size, the domain is again discretized so that the total number of grid points in both r and θ directions remain fixed at 30 at each time step. The model is explained in details elsewhere [17,6,19]. As seen in our previous experimental studies [14–16], an acoustically levitated and radiatively heated droplet undergoes rotations forming different structures. Such three-dimensional model is beyond the scope of this work.

2.5. Modeling chemical reaction

The chemical reaction of the species is triggered only when the temperature on the droplet surface exceeds 70°C. The prescribed criterion is chosen as per experimental observations in [12]. From the concentration field within the droplet, the total number of cerium nitrate particles (n_t) present in each computational cell (i, j) is calculated. The reaction is considered to occur in each cell independently without any interaction with the adjoining cells during the reaction process. The corresponding mean free path is determined as $\lambda = V_{net}/\sqrt{2}n_t\sigma.V_{net}(= V_{cell} - V_{ceria})$ is the net volume available for cerium nitrate particles present at any instant in the cell (i, j) of volume V_{cell}, excluding the volume occupied by ceria particles (V_{ceria}) and σ is the collisional cross section of the particles. In the present study, collision is considered only between cerium nitrate particles such that $\sigma = \pi d_{ppt}^2$. The rates of reaction for different cells are subsequently estimated using Eq. (17) (explained later in section 3.1.2). Since dissociation depends upon the reaction rate at any time instant, number of particles of cerium nitrate converted to ceria, n_{conv}, is calculated for every cell at different temperature ($n_{conv} = n_t e^{-r\Delta t_{vap}}$) and the sink term ($\bar{m}_1$) for cerium nitrate in Eq. (13a) is determined accordingly. It is seen from the dissociation reaction that one mole of ceria is generated per mole of cerium nitrate. Hence, the source term ($\bar{m}_2$) for ceria in Eq. (13b) is calculated from the amount of $Ce(NO_3)_3$ dissociated. From this point, the mass transport Eq. (13b) is activated and both the Eqs. (13a) and (13b) are solved for the species individually and the final concentration map ($\bar{\chi}_p$) is generated for both cerium nitrate and ceria. As per the endothermic dissociation reaction, 208 J of heat is absorbed per gram of cerium nitrate converted to ceria. Therefore, the total amount of heat absorbed ($\dot{q}_s$) is calculated based on the actual amount of species dissociated in each cell.

The experimental results [12] show the formation of bubbles, which increases the droplet size. This is due to NO_X and other gases released during reaction which gets entrapped within the droplet. In the current model, however, the gases are not allowed to expand the droplet size. The simulation is terminated when the surface concentration of ceria reaches ninety percent or when vaporized mass becomes equal to the mass of water initially present in droplet, whichever occurs earlier. The numerical model is schematically shown in Fig. 2.

3. Discussion of results

3.1. Choice of reaction rate models

3.1.1. Arrhenius and Kramers' models for chemical reaction in cerium nitrate

When a cerium nitrate droplet is heated, pure vaporization and surface regression occur first over a timescale of 10–15 s. It precipitates out of solution once the threshold temperature of 343 K is reached as per experimental observation [12]. The size of this precipitate was determined by Castillo and Munz [25] to be about 10 nm. The cerium nitrate precipitate undergoes rapid kinetic decomposition to form ceria in an endothermic reaction. The agglomeration and precipitation process occurs within a few milliseconds ($\tau \sim 2$ ms) at the end of the pure vaporization regime [17]. However the reaction timescale is about 5 s [12] which is much longer than the time period of precipitate formation and comparable to the pure vaporization regime. Hence, the process of agglomeration is not modeled in the current study and the size of cerium nitrate precipitate (r_{ppt}) is assumed to be 10–13 nm [25] at the onset of the chemical reaction process.

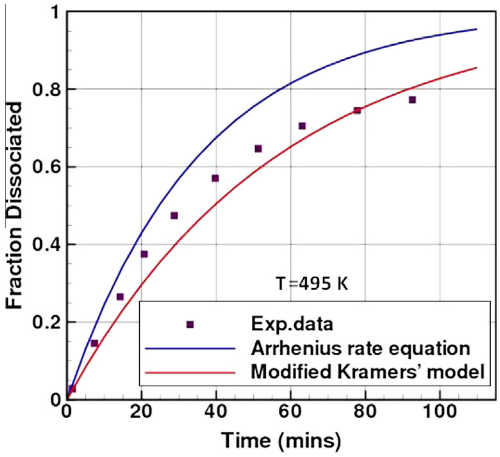

Fig. 3. Temporal evolution of cerium nitrate decomposition to ceria for a fixed ambient temperature, T = 495 K.

The rate of reaction is needed in order to understand the chemical kinetics of cerium nitrate to ceria conversion. The reaction rate in cerium nitrate can be determined using the standard Arrhenius form: $r_k = Ae^{\frac{-Ea}{RT}}$, where A is Arrhenius constant and E_a is activation energy of the reaction. The rate predicted in this particular form compared well with various experiments performed with bulk samples of cerium nitrate [10] as shown in Fig. 3. The thermal analysis was done with 15 mg of Ce $(NO_3)_3.6H_2O$ dispersed in a container and heated at a temperature range of 222°C-350°C [10]. As mentioned earlier, Saha et al. [12] showed the chemical reaction to occur at a low temperature (70°C) in about 5 s for a 500 micron levitated droplet heated by a laser heat flux of 0.45 MW/m^2. The transformation at this low temperature cannot be explained on the basis of Arrhenius form of reaction rate which is calculated to be very low and takes much longer time ($\gg 5$ s) for completion of the reaction. The reaction within a heated droplet involves spatial restriction (500 micron for the droplet in this work) which is not included in Arrhenius type of rate equation. An alternative to Arrhenius rate formulation is thus required to be used for rate determination occurring at such low temperature in a small droplet. A different analytical approach for estimating reaction rate was given by Kramers [18], which incorporates both temperature and the spatial length scales responsible for the chemical reaction included in the model.

Kramers [18] modeled chemical reaction as a stationary diffusion process when a particle in random motion in an external force field escapes a potential energy barrier and migrates from initial state A to final state B (Fig. 4). The rate of reaction was thus equivalent to corresponding rate of escape of the particle across the

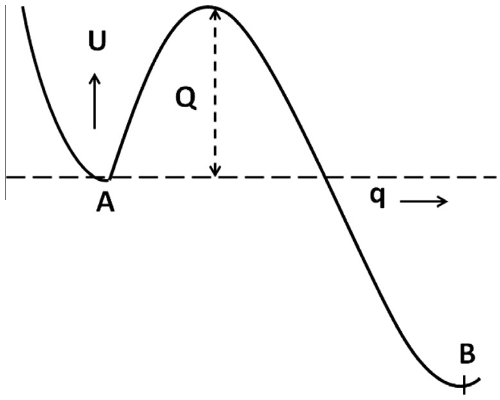

Fig. 4. Schematic of Kramers' theoretical model for reaction kinetics modeling (adopted from [18]) (reproduced with permission).

potential barrier. Assuming that the initial velocity distribution is of the Maxwell–Boltzmann type, Kramers applied Smoluchowski's diffusion equation to obtain diffusion current developed between the points A and B [18]. The reaction velocity theoretically derived by Kramers retains the classic form of Arrhenius rate equation, while the rate constant part is replaced by a frequency related variable term. The modified term is explained on the basis of Brownian motion of the particle. Potential barrier (Q) is assumed to be larger than the energy of particles (k_bT) such that a slow diffusion process (stationary diffusion current) is generated as particles move from A (present state) to B (final state) (see Fig. 4). The generalized form of reaction velocity/rate (r) derived by Kramers [18] when Brownian forces are larger than external forces:

$$r = \frac{\omega}{\eta}\sqrt{2\pi\frac{k_b}{m}T}\left\{\int_A^B e^{U/\left(\frac{k_bT}{m}\right)}dq\right\}^{-1} \tag{14}$$

where q is the spatial coordinate specifying position of the particle in potential field U (per unit mass). η is a viscosity related term given as [26]:

$$\eta = k_bT/mD \tag{15}$$

k_b is Boltzmann constant and D is the mass diffusion constant for the particle of mass m. ω is frequency factor which is defined as frequency of the particle at A [26]:

$$\omega = \frac{V}{md^2} \tag{16}$$

V is intermolecular potential energy varying over distance "d" and modeled as a harmonic oscillator.

3.1.2. Adaptation of Kramers' rate equation for a droplet

In a droplet, the chemical reaction is confined within a small volume. Accordingly, Kramers' Eq. (14) needs to be modified so that it can be applied to the droplet domain. Assuming no external energy flux to the system except the heat that is supplied from ambient through convection and the heat absorbed due to radiation, the thermal energy contributes to the excitation energy (V) required for mass m_{ppt} to undergo chemical reaction which is endothermic in nature. In a micron-sized droplet, the motion of molecules is limited within the droplet volume and hence the spatial extent (q) [$V_{drop}/N\pi\, d^2$] of a particle is considered to be its mean free path (λ) in the system. V_{drop} is the volume of the droplet while N corresponds to the total number of particles and d is the diameter of each particle. For this length scale, the potential field is assumed to be independent of λ such that the only potential barrier required for the decomposition of Ce $(NO_3)_3$ to CeO_2 is the activation energy (E). E can be obtained from Strydom and Vuuren [10]. This takes into account the effect of variation in droplet size due to the evaporation of water on the chemical reaction in terms of λ and also eliminates the integral from the velocity expression in Eq. (14). Kramers' formulation was thus modified as:

$$r = \frac{\omega}{\eta}\sqrt{2\pi\frac{k_b}{m_{ppt}}T}\{e^{E/RT}\lambda\}^{-1} \tag{17}$$

Here, $\omega = \frac{V}{m\lambda^2}$ is frequency of the particle in Brownian motion and R is the universal gas constant, E = 104 kJ/mol. For cerium nitrate to undergo transformation, 208 J of energy is required per gram of the species. Hence, energy needed for each particle, V, is calculated for conversion. Using Kramers' formulation in modified form as given by Eq. (17), the reaction rate shows dependency not only on the temperature but also on the configuration of the system in terms of λ.

The experimentally obtained loss in mass of cerium nitrate (initial mass of Ce $(NO_3)_3.6H_2O$ is 15 mg) at 495 K from [10] is added in Fig. 3. To validate the applicability of Kramers' equation in modified form for the rate calculation of the dissociation reaction, the fraction of mass of species decomposed in bulk amount of Ce $(NO_3)_3.6H_2O$ (15 mg as considered in [10]) is calculated using both the Arrhenius form of rate equation and modified Kramers' model. Here the bulk amount of Ce $(NO_3)_3.6H_2O$ is modeled as an equivalent 2.55 mm droplet in modified Kramers' model. The temperature was fixed at 495 K and no heating or vaporization was considered. The Arrhenius constant is taken as $A = 4.426 \times 10^7$ [10]. All the parameters required were estimated and the rate was plotted against time as shown in Fig. 3. The reaction rate predicted using both Arrhenius form and Eq. (17) shows similar variation with time and good agreement with the experimentally obtained data as can be seen from Fig. 3.

To show the comparison between Arrhenius rate and Kramers' models, the simulation is run for a cerium nitrate droplet (500 micron initial diameter) radiatively heated at an intensity of 0.2 MW/m^2 while the ambient is kept at 300 K. The details of the numerical model used in the simulation especially for the heat and mass transport regime have been explained earlier in section 2 . The concentration of ceria formed is calculated using both Arrhenius form of rate equation and equation (17) individually. Fig. 5 shows the total mass of ceria formed during reaction within the droplet as percentage of total mass of the droplet. The reaction is seen to be complete in a short time period of about 15 s when cerium nitrate is almost entirely converted to ceria (100% mass fraction) using modified Kramers' model. As seen in Fig. 5, the formation of ceria is not appreciable initially with Arrhenius type of model. It gradually increases with time since the rate depends only on droplet temperature. The simulation is carried up to the point till evaporation is complete. It is seen from Fig. 5, that reaction continues till about 48.8 min and only 1% mass fraction of ceria is formed. However, the experiments conducted with droplet under radiative heating [12] shows the formation of ceria at a faster rate when externally heated even with low laser irradiation (0.45 MW/m^2) and at ambient condition of 300 K. Thus, even though both models are valid for reaction rate study in bulk amount of cerium nitrate, Kramers' model is found to be better in predicting the chemical reaction within a heated droplet compared to Arrhenius rate equation which takes an impractically long time for reaction.

3.2. Validation of results

3.2.1. Validation without chemical reaction

The vaporization model is validated with the numerical work of Handscomb [27] and experimental data of Nesik and Vodnaik [28].

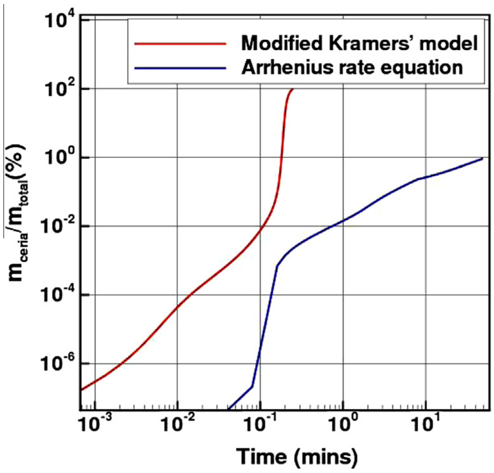

Fig. 5. Temporal variation of total mass of ceria (m_{ceria}) formed within the droplet with respect to the total mass of the droplet (m_{total}) at T_{str} = 300 K, laser power, I = 0.2 MW/m^2.

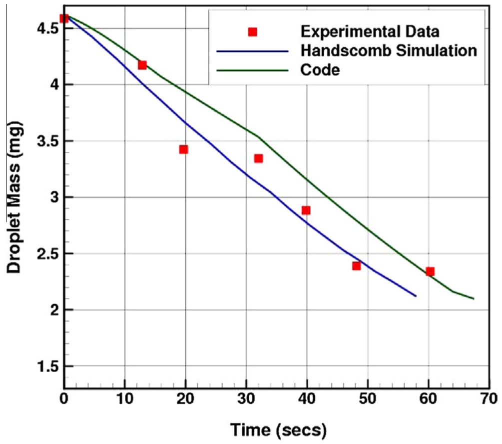

Fig. 6. Validation of the vaporization model (without any chemical reaction) with numerical data of Handscomb [27] and experimental data of Nesik and Vodnik [28] for similar heating conditions (T_{str} = 374 K, U_{str} = 1.73 m/s) and initial particle mass fraction (30 percent) [17] (reproduced with permission).

The ambient temperature was maintained at T_{str} = 374 K (without any radiative heating) and the acoustic streaming velocity at U_{str} = 1.73 m/s. The simulation was done with silica nanofluid droplet with an initial particle size of 20 nm and concentration of 30 percent. Fig. 6 shows that the vaporization model without any chemical reaction compares well with the available data in the literature [27,28].

3.2.2. Validation with chemical reaction

The vaporization model along with chemical reaction is subsequently validated with the experimental results of Saha et.al [12] for levitated droplets with radiative heating. The simulation was accomplished for an initial droplet size of 500 micron and an initial concentration of of 0.576 M cerium nitrate with an ambient temperature, T_{str} = 300 K. The laser power (I) was maintained at 0.45 MW/m^2. The temperature and dropsize regression with time at high (I = 1.8 MW/m^2) and low (I = 0.45 MW/m^2) laser powers are plotted in Fig. 7 alongside the experimental data of Saha et al. [12]. The droplet surface temperature from the numerical model compares well with the experimental data for low laser power. The numerical prediction of surface regression rate (D/D_0 plot) agrees particularly well with the experimental data [12] till about 3 s. Beyond 3 s, the experimental data show an increase of diameter due to the entrapment of gases (formed due to chemical reactions) in the droplet, which was not modeled in the current simulation.

A detailed study of the dynamics of formation of ceria is carried out for two levels of ambient temperature (425 K, 525 K) and two levels of initial mass fraction of Ce $(NO_3)_3$ (0.3 and 0.6) in water. For the droplet initial diameter of 500 microns and incident laser intensity of 0.45 MW/m^2, several cases were simulated. All the thermo physical properties (C_{pL}, ρ_L,k_L, μ_L,D_{12}) used for the simulation were adopted from [8].

3.3. Results with heat and mass transfer and chemical reaction

During its lifetime, the droplet surface temperature shows a sharp transient rise in temperature initially, a subsequent gradual decrease and finally a sharp increase with some fluctuations (more distinct at low ambient temperature) as seen in Fig. 8a. The timescale of the initial transient heating phase (about 0.4–0.5 s) varies depending upon the ambient temperature, irrespective of initial mass of Ce $(NO_3)_3$ present in the droplet. In this period, the energy supplied to the droplet by the incident laser flux and the hot convective outer flow field is used for sensible heating of the droplet since the vaporization rate is low due to low vapor pressure. Subsequently as the surface temperature of the droplet reaches the wet bulb limit, vaporization rate is augmented due to an increase in vapor pressure. The convective and radiative transfer of heat to the droplet is now completely utilized for vaporization leading to nearly a constant surface temperature with a slight decay as illustrated in Fig. 8a. At later times, rate of vaporization decreases due to an increase in solute concentration near the surface.

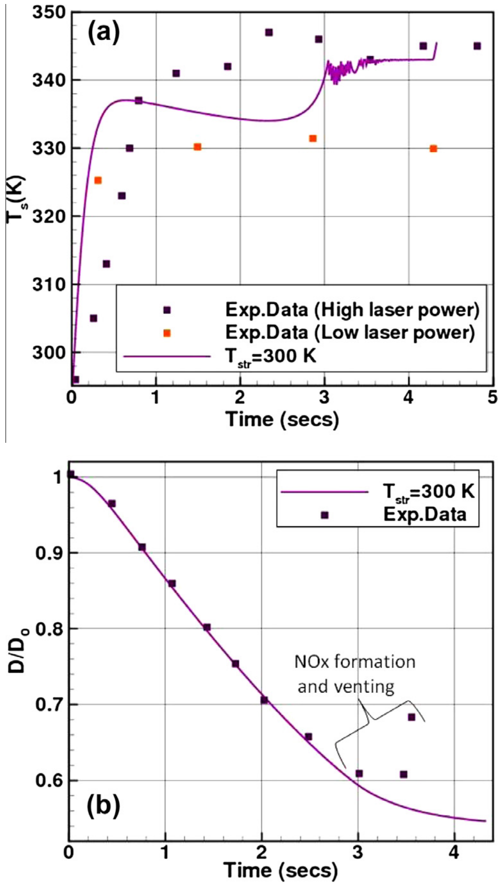

Fig. 7. Validation of numerical results with experimental datas [12] for (a) temperature at droplet surface and (b) droplet size regression rate for T_{str} = 300 K, U_{str} = 1.6 m/s, χ_i = 0.18.

Thus, continuous heating with radiation causes gradual rise in temperature and the chemical reaction is triggered once the prescribed surface temperature of 343 K is reached. With the initiation of endothermic chemical reaction, heat is absorbed for ceria formation, which causes a further drop in temperature depending upon the amount of cerium nitrate converted to ceria. The fluctuations in surface temperature (Fig. 8a) at lower ambient condition (425 K) mark the temporal variation of reaction rate depending upon the size of droplet and the temperature field. At low ambient temperature (425 K), rate of reaction is comparable to the rate of heating as seen in Fig. 9a. As a result, the temperature decreases due to reaction but immediately recuperates due to heat transfer from external modes of convection and radiation. This process continues until the reaction rate is sufficiently reduced, exhibiting undulations in temperature curve (Fig. 8a). No such oscillations in temperature are detected at T_{str} = 525 K, irrespective of cerium nitrate concentration.

With conversion of Ce $(NO_3)_3$ to CeO_2, both reaction rate and the rate of vaporization of water are reduced. The heat from the high temperature ambient and the laser flux is utilized primarily as sensible heat, raising the final temperature of the droplet (after 1.8–2.9 s of the process). Temporal variation of Ce $(NO_3)_3$ mass fraction at the droplet surface [Fig. 9b] shows a gradual rise due to

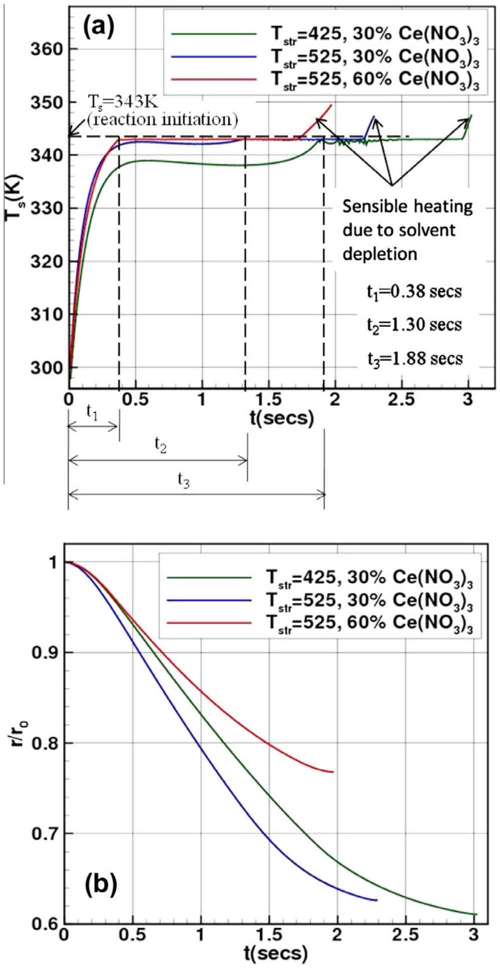

Fig. 8. Temporal variation of (a) droplet surface temperature and (b) droplet size regression rate under different heating conditions.

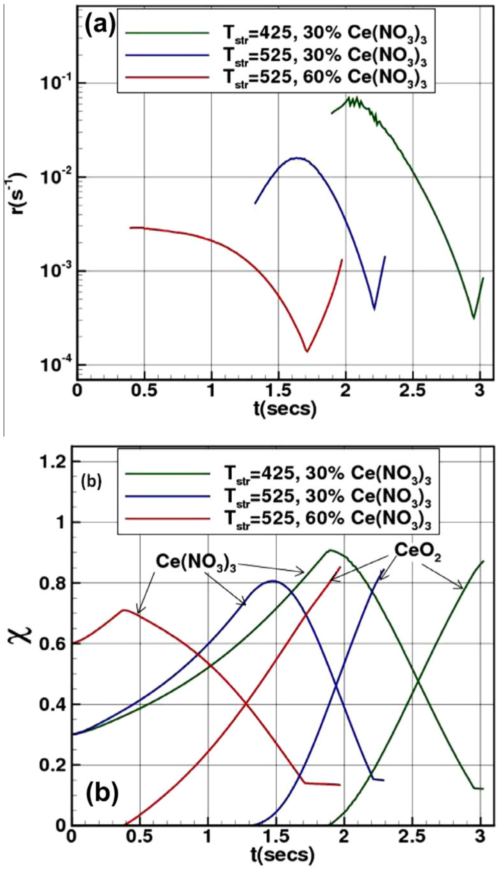

Fig. 9. Temporal variation of (a) rate of reaction and (b) mass fraction of cerium nitrate and ceria at droplet surface under different heating conditions.

vaporization of water up to a peak value till the reaction is initiated. Subsequent to the onset of reaction, the surface concentration of cerium nitrate decreases sharply as it dissociates into ceria. At this point the concentration of CeO_2 starts increasing almost linearly and continues throughout the droplet lifetime. The peak concentration of cerium nitrate at which the reaction is activated is achieved at an earlier time instant for droplets at higher ambient temperature (525 K) and higher initial mass fraction (0.6). Heating rate is high when ambient is at a higher temperature but vaporization is restricted due to the presence of undissolved Ce $(NO_3)_3$ particles. The reduction in vaporization rate due to the presence of Ce $(NO_3)_3$ is also seen in droplet size depletion curves in Fig. 8(b). Hence the heat is employed to raise the temperature of droplet and the surface specified criterion is obtained at an earlier point of time when the droplet is reduced to only about 95 percent ($t_1 = 0.38$ s). The reaction rate is a direct function of temperature and is inversely proportional to the mean free path of Ce $(NO_3)_3$ particles at any time instant. The reaction is initiated when the droplet surface is at a similar temperature in all cases. As explained previously, the presence of large number Ce $(NO_3)_3$ particles enhances the sensible heating phase of droplet and reaction is triggered when the droplet size is larger compared to a droplet with lower particle concentration. Higher concentration (initially 0.6) in larger volume creates longer mean free paths which results in a low reaction rate although temperature is high (525 K). For low ambient heating rate (425 K), temperature rises very slowly and the reaction is initiated near the later stages of droplet lifetime ($t_3 = 1.88$ s) when drop size becomes small. Within this smaller droplet volume, the mean free path is also low, resulting in a high rate of chemical reaction. As the reaction proceeds, the number of Ce $(NO_3)_3$ particles is reduced. Simultaneously, the depletion of droplet size due to vaporization of water and NO_x decreases the volume available for the particles. Thus, the mean free path of the remaining Ce $(NO_3)_3$ particles changes depending on the number of particles present and the available volume, changing the reaction rate. The reaction rate at the droplet surface shows an increase initially as droplet depletes in size, indicating a dominant effect of mean free path upon the reaction rate. As cerium nitrate is converted to ceria, mean free path increases, reducing the reaction rate. The final increase in rate is due to the sharp rise in final temperature caused by sensible heating as seen in Fig. 8(a).

The contour plots in Fig. 10 show the distribution of cerium nitrate mass fraction within the droplet just prior to the initiation of the chemical reaction. High vaporization rate and slow rate of mass diffusion result in a concentration gradient with the highest value on the droplet surface. This effect is particularly prominent for high ambient temperature (525 K). Slow vaporization at lower ambient temperature (425 K) allows sufficient time for diffusion of precipitated cerium nitrate particles within the droplet causing a more uniform distribution of mass concentration unlike the higher temperature counterpart. It is to be noted that the contour plots shown in Fig. 10 correspond to different time instants corresponding to the three cases reported here. The concentration profiles closely mimic the internal recirculation pattern due to the acoustic field particularly for the high ambient temperature case.

The contour plots in Fig. 11 show the distribution of ceria mass fraction formed after 0.5 s of the initiation of reaction inside the

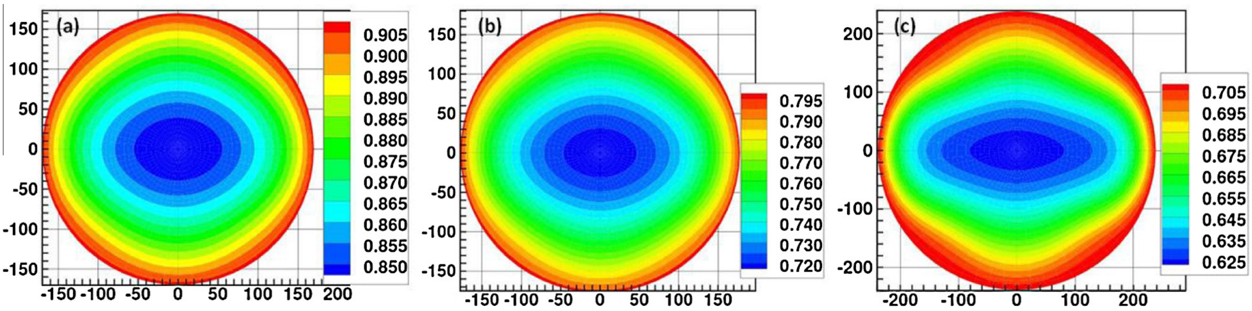

Fig. 10. Contour plots showing cerium nitrate concentration at (a) T_{str} = 425 K, U_{str} = 1.6 m/s, χ_i = 0.3 (b) T_{str} = 525 K, U_{str} = 1.6 m/s, χ_i = 0.3 and (c) T_{str} = 525 K, U_{str} = 1.6 m/s, χ_i = 0.6, just before the reaction is initiated.

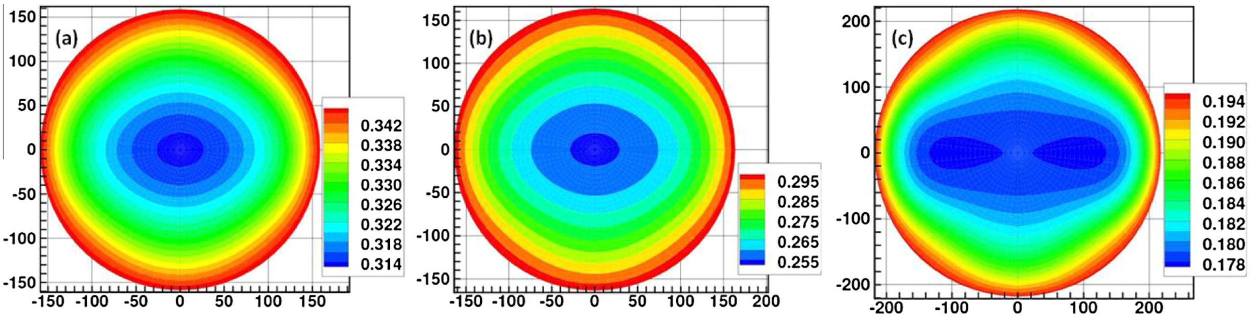

Fig. 11. Contour plots showing ceria at (a) T_{str} = 425 K, U_{str} = 1.6 m/s, χ_i = 0.3 (b) T_{str} = 525 K, U_{str} = 1.6 m/s, χ_i = 0.3 and (c) T_{str} = 525 K, U_{str} = 1.6 m/s, χ_i = 0.6, 0.5 s after the reaction is initiated.

droplet. As expected, the highest concentration of ceria is obtained at T_{str} = 425 K with an initial mass fraction of Ce $(NO_3)_3$ of 0.3 due to the high reaction rate as seen in Fig. 9(a). As per reaction, one mole of cerium nitrate (molecular weight 326 g/mol) dissociates to form one mole of ceria (molecular weight 117 g/mol). Thus, mass of Ce $(NO_3)_3$ dissociated at any instant is not equivalent to that of CeO_2 formed. As explained before, dissociation occurs at different rates for individual grids depending upon the temperature and the available mean free path. Accordingly, ceria concentration is maximum on the surface and it gradually decreases towards interior of the droplet as shown in Fig. 11. This is obvious from rate of the reaction which shows a similar variation throughout the droplet in Fig. 12 (a, b).

Temperature fields within the droplet before the reaction are shown in Fig. 13. Volumetric heat absorption due to the laser flux generates higher temperature within the droplet core with lower value at the surface due to vaporization. It is seen in Eq. (4) that temperature and mean free path are the only variables determining rate of the chemical reaction. This implies that although the temperature is higher inside the droplet, mean free path, which is a function of the concentration field and droplet size, is dominant in determining the rate of reaction. However, a reverse trend in reaction rate is seen within the droplet as shown in Fig. 12 (c) at T_{str} = 525 K and χ_i = 0.6. Comparatively higher temperature developed in the droplet core for this particular case is a more dominant factor in influencing the reaction rate which is highest at the center and gradually decreases radially outwards. Even though the formation of ceria is largest within the droplet (higher dissociation rate), a higher concentration is observed near the surface (Fig. 11(c)). This is explained on the basis of vaporization of solvent which is a surface phenomenon and increases concentration of both the species. Hence, a higher mass fraction is obtained on the surface than in the droplet core (Fig. 11(c)).

The decrease in temperature due to endothermic reaction can be observed from the temperature contours in Fig. 14. When reaction is initiated, although the surface temperature is the same for all cases, internal temperature distribution is very different. The heat absorbed depends on the number of particles of Ce $(NO_3)_3$

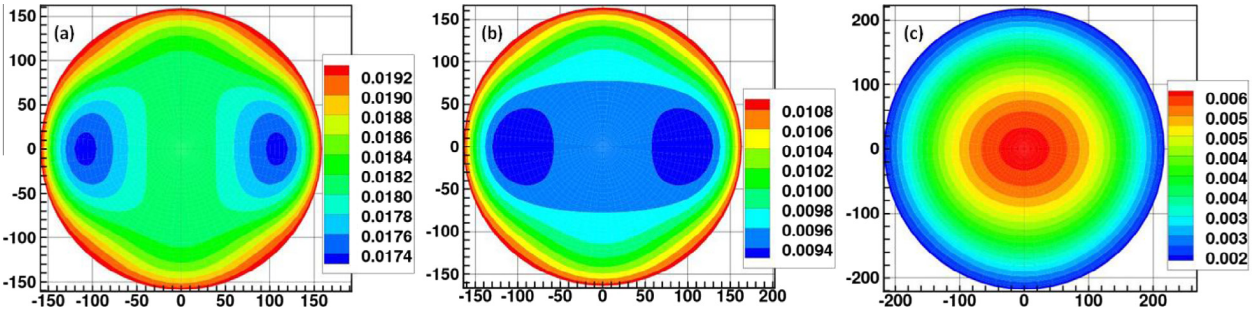

Fig. 12. Contour plots showing rate of chemical reaction within droplet at (a) T_{str}=425 K, U_{str} = 1.6 m/s, χ_i = 0.3 (b) T_{str} = 525 K, U_{str} = 1.6 m/s, χ_i = 0.3 and (c) T_{str} = 525 K, U_{str} = 1.6 m/s, χ_i = 0.6, 0.5 s after the reaction is initiated.

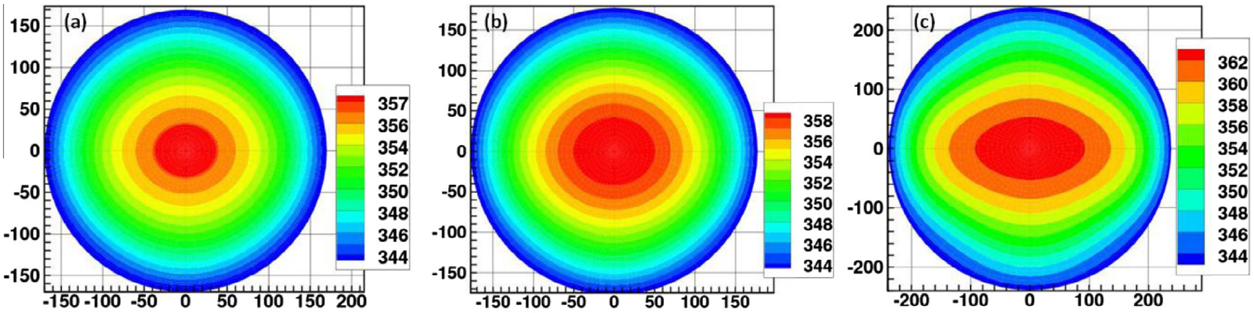

Fig. 13. Contour plots showing temperature within droplet at (a) T_{str} = 425 K, U_{str} = 1.6 m/s, χ_i = 0.3 (b) T_{str} = 525 K, U_{str} = 1.6 m/s, χ_i = 0.3 and (c) T_{str} = 525 K, U_{str} = 1.6 m/s, χ_i = 0.6, just before the reaction is initiated.

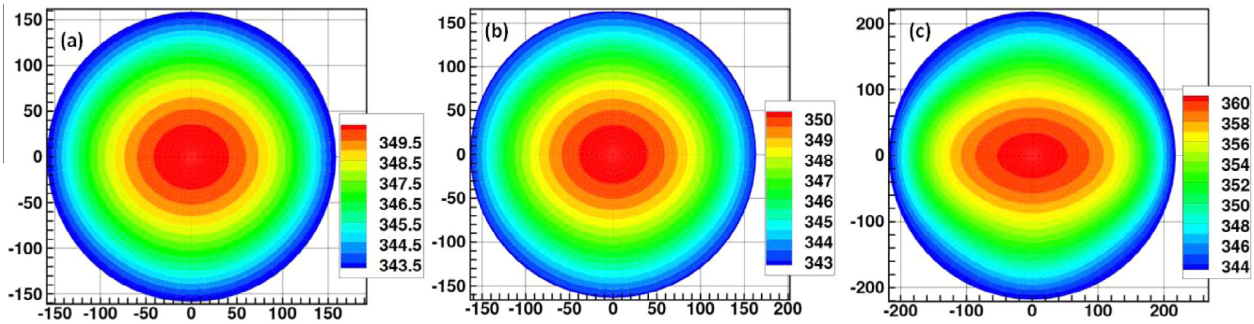

Fig. 14. Contour plots showing temperature within droplet at (a) T_{str} = 425 K, U_{str} = 1.6 m/s, χ_i = 0.3 (b) T_{str} = 525 K, U_{str} = 1.6 m/s, χ_i = 0.3 and (c) T_{str} = 525 K, U_{str} = 1.6 m/s, χ_i = 0.6, 0.5 s after the reaction is initiated.

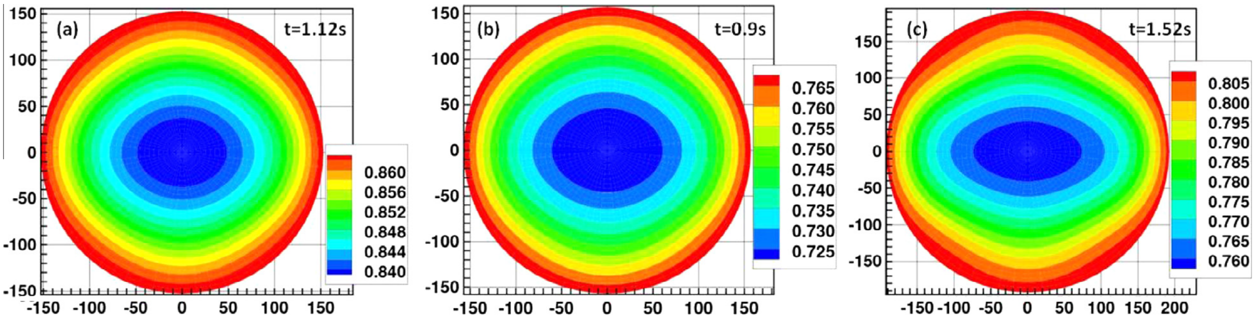

Fig. 15. Contour plots showing ceria within droplet at (a) T_{str} = 425 K, U_{str} = 1.6 m/s, χ_i = 0.3 (b) T_{str} = 525 K, U_{str} = 1.6 m/s, χ_i = 0.3 and (c) T_{str} = 525 K, U_{str} = 1.6 m/s, χ_i = 0.6, at the final time step of reaction.

dissociating into CeO_2 and the cell temperature. Accordingly, temperature decrease is expected to be higher towards the interior of the droplet due to higher dissociation rate. However, continuous heating from hot ambient and the incident laser flux counteracts the drop in temperature. The lifetime of droplet varies under different heating conditions depending upon the reaction rate and the rate of vaporization. Fig. 15 demonstrates the concentration field developed within the droplet at the final time step of the entire process. For the same initial Ce $(NO_3)_3$ concentration (χ_i = 0.3), since the surface is at same temperature (343 K), the volume of droplet and the number of particles are favorable for reaction at lower ambient temperature. As predicted, a higher dissociation of cerium nitrate is obtained at T_{str} = 425 K (initial mass fraction = 0.3). Consequently, mass fraction of ceria is highest at T_{str} = 425 K as seen in Fig. 15. It is also noted that at T_{str} = 525 K, ceria concentration exhibits a higher value for higher initial Ce $(NO_3)_3$ concentration (0.6). This is due to the longer time it takes to react (t = 1.52 s) as compared to that at χ_i = 0.3 (t = 0.9 s). Hence it is seen that if the timescale is not restrained, maximum amount of ceria can be obtained even with a low initial concentration of cerium nitrate if ambient heating is maintained at a lower temperature. Same inference is true for a higher initial particle concentration if ambient is at a comparatively higher temperature.

The entire process flow is schematically shown in Fig. 16. The various events occurring in the droplet lifecycle while being heated is summarized chronologically. The heat absorbed by the droplet causes immediate rise in temperature and liquid phase vaporization, resulting in regression of the droplet size that continues throughout the process. The vaporization is followed by surface accumulation (Fig. 16 (b)) and precipitation of cerium nitrate (Fig. 16 (c)). The concentration of cerium nitrate thus increases with time (t_v) (Fig. 16 (d)). Heating continues throughout the process and the reaction is triggered when the specified condition of 343 K is attained. For instance, at T_{str} = 425 K, Fig. 16(d) represents the distribution of Ce $(NO_3)_3$ throughout the droplet at t3 = 1.88 s (as shown in Fig. 10(a)). As time elapses, conversion of Ce $(NO_3)_3$

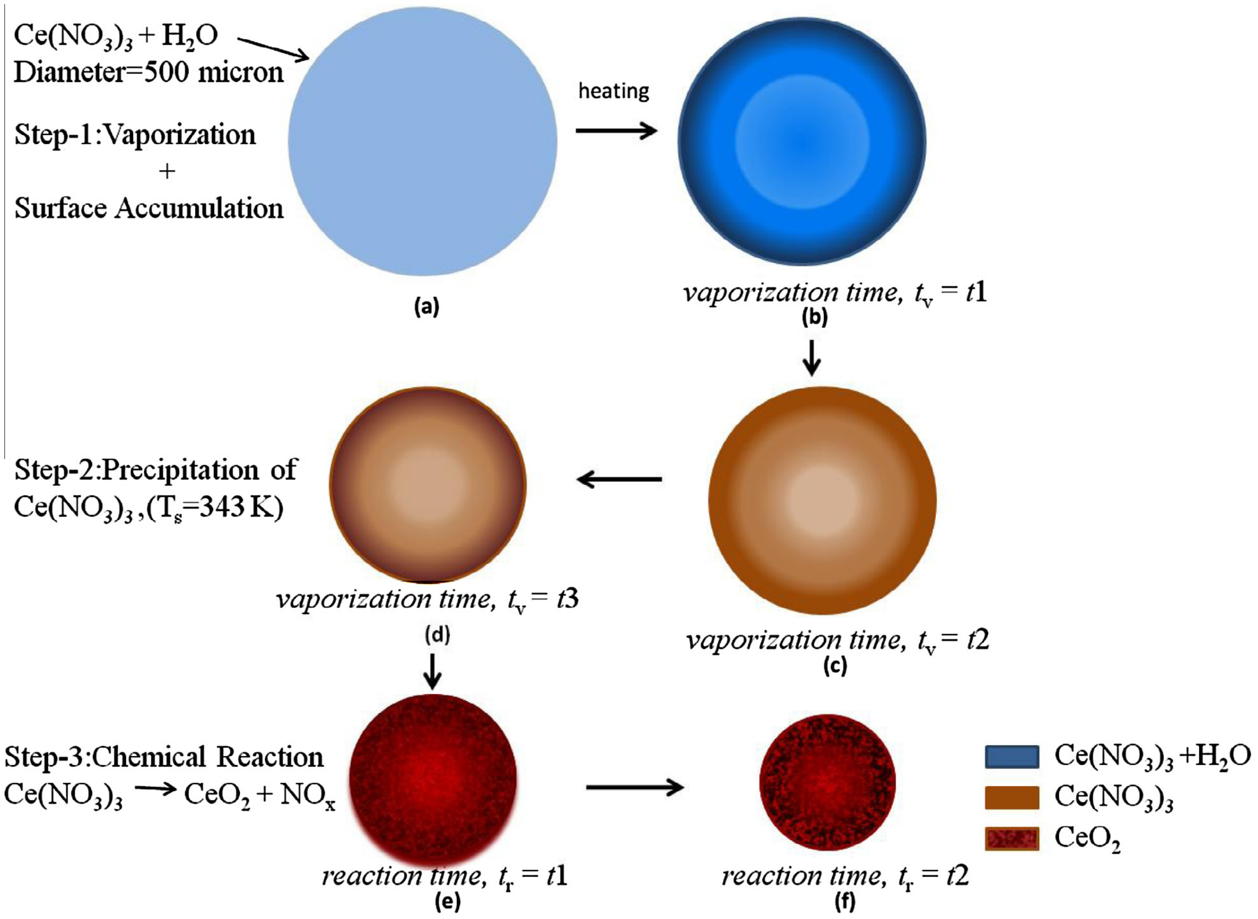

Fig. 16. The chronology of different processes in droplet lifetime.

to CeO_2 and vaporization of water increases the concentration of ceria within the droplet ($t_r = 1.12$ s) which is explained in Fig. 15(a). Fig. 16 shows complete conversion of cerium nitrate to ceria if the external heating is continued to the end of simulation. However, the entire amount of cerium nitrate may not undergo reaction as observed in the experiments, where the laser is turned off before completion of the process.

4. Conclusions

A numerical model has been established to understand the thermo-physical and chemical transformation in an acoustically levitated hydrated cerium nitrate droplet subjected to radiative and convective heating. The model uniquely combines a 2D transient multispecies heat and mass transport equation for the vaporizing droplet with detailed chemical kinetics of cerium nitrate decomposition to ceria. The formation of ceria from the dissociation of cerium nitrate occurs at low temperature and is illustrated with Kramers' rate equation which is modified appropriately for droplets. The vaporization model inclusive of chemical kinetics validates the experimental results obtained with radiatively heated aqueous cerium nitrate droplets found in literature. The amount of cerium nitrate converted to ceria can be spatially predicted with the proposed model. Reaction rate can be easily adjusted by controlling the temperature, concentration of cerium nitrate and size of the droplet. The drop size and the cerium nitrate concentration have greater influence on the rate of the dissociation reaction. It is seen that the timescale of reaction and rate of vaporization are also important in order to determine the mass fraction of ceria formed at different time instants in the droplet lifecycle. The contours of ceria formation suggest higher concentration near the droplet surface.

References

[1] S. Patil, S.C. Kuiry, S. Seal, Nanocrystalline ceria imparts better high-temperature protection, Proc. R. Soc. Lond. A 460 (2004) 3569–3587.
[2] V. Viswanathan, R. Filmalter, S. Patil, S. Deshpande, S. Seal, High-temperature oxidation behavior of solution precursor plasma sprayed nanoceria coating on martensitic steels, J. Am. Ceram. Soc. 90 (3) (2007) 870–877.
[3] B. Abramzon, W.A. Sirignano, Droplet vaporization model for spray combustion calculations, Int. J. Heat Mass Transfer 32 (9) (1989) 1605–1618.
[4] H. Jia, G. Gogos, High pressure droplet vaporization effects of liquid-phase gas solubility, Int. J. Heat Mass Transfer 36 (18) (1993) 4419–4431.
[5] M. Renksizbulut, R.J. Haywood, Transient droplet evaporation with variable properties and internal circulation at intermediate Reynolds numbers, Int. J. Multiph Flow 14 (2) (1988) 189–202.
[6] A. Ozturk, B.M. Cetegen, Modeling of plasma assisted formation of precipitates in zirconium containing liquid precursor droplets, Mat. Sci. Eng. A 384 (2004) 331–351.
[7] S. Basu, B.M. Cetegen, Modeling of thermophysical processes in liquid ceramic precursor droplets heated by monochromatic irradiation, J. Heat Transfer 130 (071501) (2008) 1–8.
[8] A. Saha, S. Seal, B. Cetegen, E. Jordan, A. Ozturk, S. Basu, Thermo-physical processes in cerium nitrate precursor droplets injected into high temperature plasma, Surf. Coat. Technol. 203 (2009) 2081–2091.
[9] F. Vratny, S. Kern, F. Gugliotta, The thermal decomposition of cerium (III) nitrate hydrate, J. lnorg. Nu¢l. Chem. 17 (1961) 281–285.
[10] C.A. Strydom, C.P.J. van Vuuren, The thermal decomposition of cerium (III) nitrate, J. Therm. Anal. 32 (1987) 157–160.
[11] A. Saha, V. Singh, S. Seal, S. Basu, Vaporization and precipitation characteristics of cerium nitrate precursor droplets heated by monochromatic irradiation, Surf. Coat. Technol. 203 (2009) 2102–2115.
[12] A. Saha, S. Basu, C. Suryanarayana, R. Kumar, Experimental analysis of thermo-physical processes in acoustically levitated heated droplets, Int. J. Heat Mass Transfer 53 (2010) 5663–5674.
[13] W.W. Wendlandt, The thermolysis of the rare earth and other metal nitrates, Anal. Chem. Acta 15 (1956) 435–439.

[14] A. Saha, S. Basu, R. Kumar, Particle image velocimetry and infrared thermography in a levitated droplet with nanosilica suspensions, Exp. Fluids 52 (2012) 795–807.

[15] A. Saha, S. Basu, R. Kumar, Effects of acoustic streaming-induced flow in evaporating nanofluid droplets, J. Fluid Mech. 692 (2012) 207–219.

[16] R. Kumar, E. Tijerino, A. Saha, S. Basu, Structural morphology of acoustically levitated and heated nanosilica droplet, Appl. Phys. Lett. 97 (123106) (2010) 1–3.

[17] B. Pathak, P. Deepu, S. Basu, R. Kumar, Modeling of agglomeration inside a droplet with nanosuspensions in an acoustic field, Int. J. Heat Mass Transfer 59 (2013) 161–166.

[18] H.A. Kramers, Brownian motion in a field of force and diffusion model of chemical reactions, Physica VII (4) (1940) 284–304.

[19] W.A. Sirignano, Fluid Dynamics and Transport of Droplets and Sprays, second ed., Cambridge University Press, New York, 2010.

[20] A.Y. Rednikov, H. Zhao, S.S. Sadhal, E.H. Trinh, Steady streaming around a spherical drop displaced from the velocity antinode in an acoustic levitation field, Q. J. Mech. Appl. Math. 59 (3) (2006) 377–397.

[21] M.C. Yuen, L.W. Chen, On drag of evaporating liquid droplets, Combust. Sci. Technol. 14 (1976) 147–154.

[22] B. Abramzon, S. Sazhin, Convective vaporization of a fuel droplet with thermal radiation absorption, Fuel 85 (2006) 32–46.

[23] G.L. Hubbard, V.E. Denny, A.F. Mills, Droplet evaporation: effects of transients and variable properties, Int. J. Heat Mass Transfer 18 (1975) 1003–1008.

[24] R. Clift, J.R. Grace, M.E. Weber, Bubbles Drops and Particles, Academic Press, New York, 1978.

[25] I. Castillo, R.J. Munz, Transient modeling of heat, mass and momentum transfer of an evaporating cerium nitrate solution droplet with a surrounding shell in a rf thermal argon–oxygen plasma under reduced pressure, Int. J. Heat Mass Transfer 50 (2007) 4468–4487.

[26] B. Gavish, Position-dependent viscosity effects on rate coefficients, Phys. Rev. Lett. 44 (17) (1980) 1160–1163.

[27] C.S. Handscomb, Ph.D. thesis, Simulating droplet drying and particle formation in spray towers, Cambridge University (2008).

[28] S. Nesik, J. Vodnik, Kinetics of droplet evaporation, Chem. Eng. Sci. 46 (1991) 527–537.